Journal of Hazardous Materials 408 (2021) 124976

Contents lists available at ScienceDirect

Journal of Hazardous Materials

journal homepage: www.elsevier.com/locate/jhazmat

Rationally designed dipicolinate-functionalized silica for highly efficient recovery of rare-earth elements from e-waste

Olena Artiushenko [a], Vladimir Zaitsev [a,b,*], Wendy S. Rojano [a], Gabriel A. Freitas [a], Michael Nazarkovsky [a], Tatiana D. Saint'Pierre [a], Jiang Kai [a]

[a] Pontifical Catholic University of Rio de Janeiro, Marquês de São Vicente St. 225, Rio de Janeiro 22451-900, Brazil
[b] National University of Kyiv-Mohyla Academy, 2 Skovorody vul., Kyiv 04070, Ukraine

ARTICLE INFO

Editor: Dr. Rinklebe Jörg

Keywords:
Surface-assembling synthesis
Dipicolinic acid
Rare-earths elements
Fluorescent lamp waste
Dispersive SPE

ABSTRACT

Composition of the immobilized layer plays a crucial role in metal adsorption properties of complexing organo-mineral materials. Ignoring the specific features of chemical reactions on solid surface can lead to a significant deterioration in the target properties of the resulted materials. In this research we demonstrated that rationally designed surface-assembling synthesis of organo-silica with covalently immobilized fragments of dipicolinic acid (DPA) resulted in the adsorbent that is capable quantitively recover almost all Rare Earth elements (REEs) from multielement solution with pH > 1.7. In ten consecutive adsorption/desorption cycles no noticeable loss of its efficiency was found, with a mean value of REEs recovery larger than 97%. The adsorbent has been used to recover REEs from model solutions (22 metal ions in 0.5 mol L^{-1} NaCl) and real leaching solution of waste of fluorescent lamps. It was demonstrated that even 3200-fold excess of Fe and Cu ions only slightly reduces REEs recovery. The adsorbent is capable to recover above 80% of all (except La) REEs from acidic leaching solution from fluorescent lamps with enrichment factors above 600. After adsorption of Eu^{3+} and Tb^{3+}, the resulting materials exhibited strong red and green luminescence, respectively, indicating chelating mechanism of REEs adsorption on SiO_2-DPA.

1. Introduction

In 21 century REEs have received diverse of applications as components in high technology devices, including smartphones, digital cameras, computer hard disks, fluorescent and light-emitting-diodes, flat-screen televisions, etc.(Dushyantha et al., 2020; Jyothi et al., 2020; Pagano et al., 2019). Therefore, European Commission included REEs to the list of most critical mineral raw materials that are an essential part of both high-tech products and every-day consumer products. According to the latest report, 95% of REEs are produced in China with only 3 – 8% of end-of-life recycling input rate (European Commission, 2017). Due to a recent high-tech boom with extensive utilization of REE, the amount of REE-containing electronic waste (e-waste) products is growing every year. Thus, the time when alternative sources of REEs will become an important issue is approaching very quickly (Ambaye et al., 2020; Gaustad et al., 2020; Jyothi et al., 2020; Swain and Mishra, 2019). For example, Brazil annually generates about 1.5 million tons of e-waste (Ottoni et al., 2020). Today there are three major applications of REEs that represent more than 80% of the rare-earth market: permanent magnets (38%), lamp phosphors (32%) and rechargeable batteries (13%) (Binnemans et al., 2013). Thus, it can be assumed that these wastes are the most promising alternative source of REEs.

The problem of e-waste recycling already attracts considerable attention of scientists and industry and it is expected that in long-term global demand for REEs, environmentally sustainable production process shall substitute or supplement current ore sources (Dutta et al., 2016). Besides the intrinsic value as a secondary source of REEs, potentially reducing the consumption of primary raw materials, geopolitical factors make e-waste recycling even more important (European Commission, 2017). Hydrometallurgical and pyrometallurgical techniques are the two most commonly used in REEs recycling techniques (Omodara et al., 2019). Most common hydrometallurgical techniques include dissolving of e-waste in mineral acids (leaching) with further precipitation, solvent extraction (Gergoric et al., 2017), ion exchange (Chour et al., 2018) or adsorption of the target ions (Ambaye et al., 2020; Pramanik et al., 2020). Since solvent extraction is the only

* Corresponding author at: Pontifical Catholic University of Rio de Janeiro, Marquês de São Vicente St. 225, Rio de Janeiro 22451-900, Brazil.
E-mail addresses: vnzaitsev@puc-rio.br, zaitsev@univ.kiev.ua (V. Zaitsev).

https://doi.org/10.1016/j.jhazmat.2020.124976
Received 7 October 2020; Received in revised form 18 December 2020; Accepted 23 December 2020
Available online 28 December 2020

technology used in mining production, there is a great desire to adapt it for e-waste processing. Unfortunately, REEs separation based on solvent extraction utilizes a lot of toxic and corrosive organic solvents and generates large amounts of waste. Thus, it is not acceptable for installation in urban sites where e-wastes have been generated. Contrary to solvent extraction, solid-phase extraction (SPE) is much more environmentally friendly and more cost-effective. It also offers high enrichment factor, easy and rapid operation. Thus, a lot of attention was paid to the development of SPE technologies for REEs recycling (C.E.D. Cardoso et al., 2019a, 2019b; Hu et al., 2018; Mosai et al., 2019; Pereao et al., 2018; Pramanik et al., 2020; Swain and Mishra, 2019). The adsorbent plays a key role in SPE-based methodology. The ideal SPE adsorbents are expected to feature with the following characteristics: large specific surface area, high chemical and mechanical stability, fast kinetics of adsorption and desorption, reversible adsorption, high selectivity and recovery rate (Hu et al., 2016). Besides the conventional materials, such as activated carbon and alumina (Celso E. D. Cardoso et al., 2019a, 2019b), a variety of novel materials including ion-imprinted polymers, restricted access materials, and metal-organic frameworks have been employed as the adsorbents for solid-phase extraction of REEs (Hu et al., 2016). Mesoporous silicas with immobilized metal-binding ligands meet the requirements for SPE recovery of REEs (Pinta, 2017; Pyrzynska et al., 2016). The silica gel matrix ensures a large surface area of the adsorbent and its high kinetic characteristics, and the immobilized ligands provide the required selectivity and affinity to REEs. Among a variety of ligands, those that form stable complexes with REE are in focus. For example, silica-based adsorbents with immobilized fragments of polydentate aminocarboxylates (Lerner et al., 2019; Zhang et al., 2016), aminophosphonates (Olena Artiushenko et al., 2020a, 2020b; Callura et al., 2018; Noack et al., 2016) and hydroxamates (O. Artiushenko et al., 2020a, 2020b) were successfully used for preconcentration of REEs (Iftekhar et al., 2018). Even though derivatives of 2,6- pyridinedicarboxylic acid (dipicolinic acid, DPA) have widely been used in the chemistry of REEs (see, for example (Barja et al., 2011)), adsorption properties of silica-based material with this immobilized DPA toward REEs have not yet been studied.

Several attempts have been made to immobilized DPA on silica surface. For example, 2,6-pyridinedicarboxylate derivative was attached to mesoporous silica surface by thermal treatment of SBA-15 with N^2,N^6-bis(2-hydroxyethyl)pyridine-2,6-dicarboxamide (Fig. 1b) (Li et al., 2015). However, this approach leads to the formation of hydrolytically unstable Si-O-C bond (see, for example (Engelhardt, 1979)) and thus cannot be recommended for recovery of REES from water media. Silica-based adsorbents with DPA fragments were also obtained in sol-gel synthesis by hydrolysis of N,N-bis(trimethoxysilylpropyl)−2, 6-pyridine dicarboxamide (Fig. 1c) (Franville et al., 2001; Verma and Dubey, 2020; Yuan et al., 2015).

In contrast to earlier published approaches, in this research, mesoporous silica-based adsorbent with covalently immobilized fragments of 2,6-pyridinedicarboxylic acid (SiO_2-DPA) has been obtained by surface assembling. Special attention was paid to the synthetic procedure, which allows one to bind the target ligand bounded with the carrier surface via only one carboxylic group (Fig. 1d).

Information about application of DPA-containing adsorbents for recovery of metal ions is very limited. For example, silica-immobilized DPA has been applied for Hg(II) and some other heavy metal preconcentration (Yuan et al., 2015; Zajtsev et al., 2004). In the only publication where DPA-containing adsorbent has been used for REEs preconcentration, it was reported the application of Amberlite XAD-4 with immobilized 2,6-diacetylpyridine (Fig. 1a) for preconcentration of rare earth elements from seawater (Karadaş et al., 2011). However, the adsorbent demonstrated poor REEs retention and limited pH-range of the adsorbent efficiency. For example, recovery of Nd, Ho, Ce and Sm were five times smaller than La, Lu and Yb and optimal conditions for REEs adsorption were achieved in solution with pH >5.0 (Yuan et al., 2015). Poor adsorption properties of earlier reported DPA-based adsorbents towards REEs might be related to the fact that DPA fragments on such adsorbents have been attached to the support by means of two carboxylic groups (Fig. 1a-c) that can accentually reduce stability of metal complexes and thus affinity of the immobilized ligand towards REEs (Yuan et al., 2015).

In this research, adsorption properties toward REEs of SiO_2-DPA obtained by surface assembling approach have been investigated. The recovery of REEs from multielement solution and also in the presence of 22 interfering metal ions has been studied, as well as metal adsorption isotherms, adsorption kinetics and SiO_2-DPA reusability. The adsorbent was successfully applied for selective recovery of rare earth elements from acidic leaching solution of waste fluorescent lamps.

2. Experimental section

2.1. Chemicals

Silica gel (pore size 60 Å, 40–63 μm particle size, surface area 460–580 m^2g^{-1}), (3-Aminopropyl)triethoxysilane (APTES, ≥98%), 2,6-pyridinedicarbonyl dichloride (≥97%), N,N-Diisopropylethylamine (DIPEA, 99.5%) were purchased from Merck; toluene (99.9%), ethanol (99.8%); europium(III) chloride hexahydrate (≥99.9%), terbium(III) chloride hexahydrate (99.9%); nitric acid (ACS reagent, 70%) and hydrochloric acid (ACS reagent, 37%) were supplied from Merck; ICP metal standard solutions: a) multielement solution of 16 REEs with concentration of each metal 100 mg L^{-1}, b) multi-element standard solution IV (22 metals in 6% HNO_3 with concentration of each metal 1000 mg L^{-1}), c) Fe(III) and Cu(II) standard solutions with

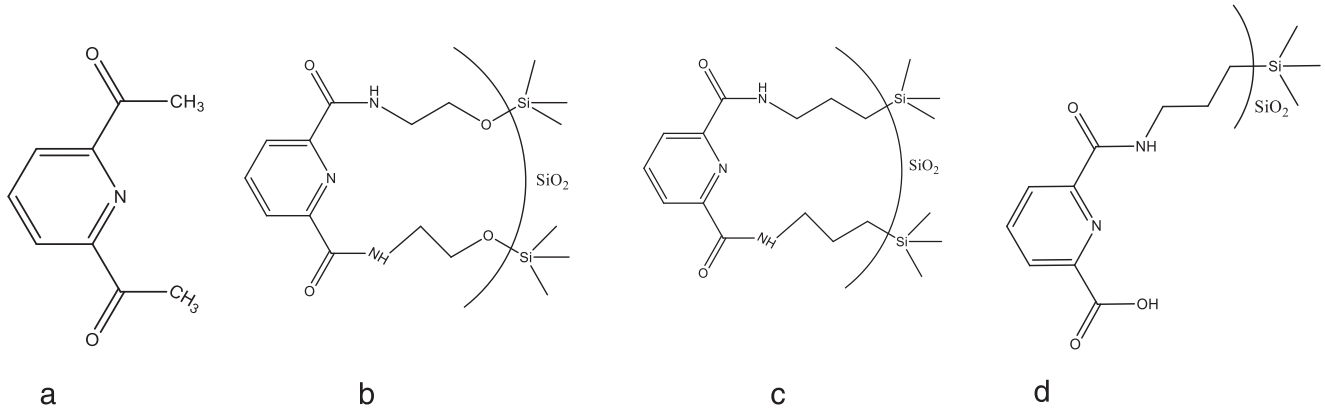

Fig. 1. Schematic illustration of immobilized layer composition on XAD-4 (a), SBA-15 (b), mesoporous silica (c), and currently reported (d) adsorbents, containing 2,6-pyridinedicarboxylic derivatives.

concentration 1000 mg L^{-1} - all were obtained from Merck. Toluene was used after drying with calcium hydride. Before modification, silica gel was refluxed in 0.1 mol L^{-1} HNO_3 to remove metal impurities and dried in muffle at 550 °C for 6 h. APTES was distilled in a vacuum before utilization. Other chemicals were utilized as received.

The lamp phosphor residue was obtained from an authorized waste repository for discarded lamps at Pontifical Catholic University of Rio de Janeiro, Brazil.

Stock solutions of europium (III) and terbium (III) (1000 mg L^{-1}) were prepared by dissolving a weighed quantity of their chlorides in distilled water. The working solutions of desired concentrations were prepared by serial dilution of stock solutions or ICP standards. Ultrapure water obtained from a Milli-Q system was used for the preparation of all types of water solutions.

2.2. Syntheses of SiO_2-DPA

Surface functionalization of silica gel with 2,6-pyridinedicarbonyl dichloride.

At the first stage, silica gel was modified with aminopropyl groups - SiO_2-$(CH_2)_3$-NH_2 - by treatment with (3-aminopropyl)triethoxysilane in absolute toluene. At the second stage, 0.42 g of 2,6-pyridinedicarbonyl dichloride was mixed with 1.2 mL of N,N-diisopropylethylamine and 100 mL of acetonitrile in a round bottom flask equipped with a mechanical stirrer. Then 1 g of obtained amino silica gel was added under rapid stirring. The reaction was kept under stirring for 4 h at room temperature. Then, the solid phase was separated by filtration, washed with acetonitrile and transferred to a Becker and sodium acetate buffer (pH = 6.0) was added for next 24 h for hydrolysis of anhydride. The resulted adsorbent (SiO_2-DPA) was separated by filtration, washed in a Soxhlet apparatus with acetonitrile for 24 h and ethanol for further 12 h and dried at 120 °C for 8 h under vacuum. Scheme of SiO_2-DPA preparation is shown in Fig. 2.

2.3. Characterization

FTIR spectra of samples were recorded on FTLA-2000 spectrometer. Textural properties were analyzed using low-temperature nitrogen adsorption-desorption (Micrometrics ASAP 2020). The total pore volume, V_p, was determined at the maximal adsorption ($p/p_o \approx 0.99$). As for the specific surface area, S_{BET}, this parameter was evaluated via standard BET method. The pore size distribution (dV/dx, PSD_V) and average pore radius (R_{ave}) were estimated through two approaches for cylindrical pores – modified Nguyen-Do (MND) (Gun'ko, 2014) and equilibrium model of nonlocal DFT (NLDFT) (Landers et al., 2013). CHN elemental analyses were performed on PE-2400 (Perkin Elmer). Thermogravimetric analyses were made on a Pyris 1 TGA (Perkin Elmer). The surface composition was studied by X-ray photoelectron spectroscopy (XPS) using a K-Alpha X-ray photoelectron spectrometer (Thermo Scientific). The surface morphology of neat and modified silica gel particles was observed with scanning electron microscopy, SEM (JEOL JSM 6490 LV). Luminescent properties of functionalized materials were studied using TGM (Toroidal Grating Monochromator) beamline with an energy range of 3–330 eV (400–4 nm) in Brazilian Synchrotron Light Laboratory. The concentrations of metal ions were determined by inductively coupled plasma mass spectrometry (ICP-MS) model Nexlon 300X, and inductively coupled plasma optical emission spectrometry (ICP-OES) model Optima 7300 DV, both from Perkin Elmer.

2.4. Adsorption studies

The adsorption and desorption experiments were performed in a dispersive SPE mode. For this, 10 mg of the adsorbent samples were dispersed in 10 mL of working solution, prepared from ICP standard solution of REEs. The working solution of competitive ions was also added for some experiments at the desired concentrations. The suspension pH was adjusted using 0.1–1.0 mol L^{-1} HNO_3, and then, they were shaken for 0.5–30 min in the falcon tubes. After adsorption equilibrium has been reached, the acidity of the suspensions was measured by pH-meter, 5 mL of the solutions were filtered through a 0.45 μm membrane and analyzed by inductively coupled plasma mass spectrometry (ICP-MS) or inductively coupled plasma atomic emission spectroscopy (ICP-OES). Adsorption of metals (A, %) was determined from five parallel experiments and calculated from Eq. (1):

$$A, \% = \frac{(C_i - C_e) \times 100}{C_i}, \quad (1)$$

where C_i, C_e – initial and equilibrium concentration of metal ion solution in the aqueous phase, in μg L^{-1}.

Desorption experiments were realized using metal-containing samples of SiO_2-DPA obtained after the adsorption experiments. To do this, each sample was initially rinsed with distilled water with pH= 3.0 and then 10 mL 2.0 mol L^{-1} HNO_3 solution was added. The suspensions were left in a shaker for 15 min, and then, the concentrations of metals in the supernatant were determined by ICP-MS. The elution degree (E, %) was determined from five parallel experiments and calculated from Eq. (2):

$$E, \% = \frac{C_e \times 100}{C_i}, \quad (2)$$

The overall recovery of the REEs from solution on SiO_2-DPA was determined from subsequent adsorption and desorption experiments and calculated from Eq. (2). The adsorbent reusability was determined from ten subsequent adsorption/desorption experiments using the same sample of SiO_2-DPA. After each cycle, the adsorbent was separated by centrifugation and rinsed with water. The supernatant was analyzed by ICP-MS on metal content. The results of the investigation were presented as a violin plot of metal recovery.

For the investigation of REEs adsorption versus pH, the multielement

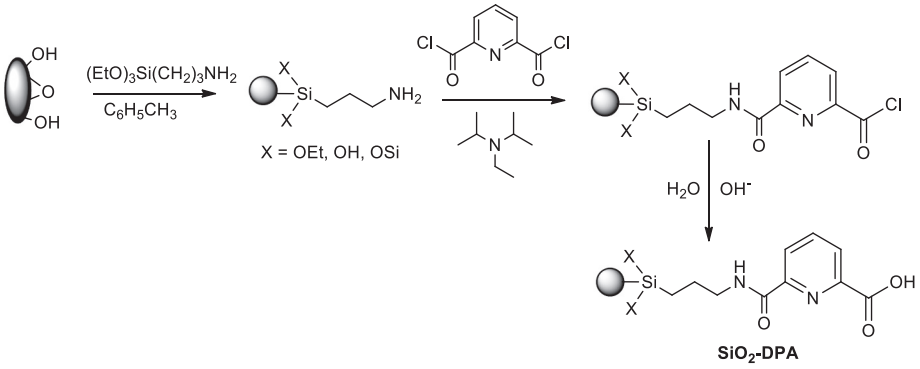

Fig. 2. General scheme of SiO_2-DPA synthesis by surface assembling.

solution has been used with a concentration of each REE ion - 20.0 μg L^{-1} and concentration of Ca^{2+} ion - 1.0 mg L^{-1} in the pH range 1–7.

The rate of adsorption was studied for Eu^{3+} solution with pH= 3.0 and concentration 10 mg L^{-1}. Adsorption isotherms were obtained from experiments were samples of SiO_2-DPA (10 mg) were immersed to 10 mL solution of Eu^{3+} with pH = 3.0. The concentration of Eu in the solutions was varied from 0.1 to 25 mg L^{-1}. The equilibrium adsorption capacity (q_e) and the capacity of the adsorbent at time t (q_t) were calculated from Eq. (3):

$$q = \frac{(C_i - C_e) \times V}{m}, \quad (3)$$

where: V – volume of the solution (L); m – adsorbent mass (g).

Distribution coefficients (K_d) of REEs between liquid and solid phases were calculated from Eq. (4):

$$K_d = \frac{(C_i - C_e)}{C_e} \times \frac{V}{m}, \quad (4)$$

Interference of foreign ions on REEs recovery has been studied using two types of model solutions. The first type (solution A) contained Fe^{3+} and Cu^{2+} ions. The second type (solution B) contained 22 metal ions (Ag^{+}, Al^{3+}, Ba^{2+}, Bi^{3+}, Ca^{2+}, Cd^{2+}, Co^{2+}, Cr^{3+}, Cu^{2+}, Fe^{3+}, Ga^{3+}, In^{3+}, K^{+}, Li^{+}, Mg^{2+}, Mn^{2+}, Na^{+}, Ni^{2+}, Pb^{2+}, Sr^{2+}, Tl^{3+} and Zn^{2+}). In the interference experiment, the mass of the adsorbent has kept constant (10 mg) as well as the concentration of each REE (20.0 μg L^{-1} and 100.0 μg L^{-1} for interfering solution A and B, correspondingly), while the concentration of interfered ions was varied from 1 to 32 mg L^{-1}. The interference effect of 22 metal ions was studied in constant ionic strength created by 0.5 mol L^{-1} NaCl.

Leaching solution of waste fluorescent lamps has been prepared in the next steps. First, waste fluorescent powder from tubular lamps of different manufacturers was sieved to separate the powder from the glass and dried at 110 °C in vacuum for 2 h using cartridge filled with sulfur powder. Then 0.5 g of waste phosphor powder was treated with 2.5 mL of aqua regia at 80 °C under stirring for 2 h. Finally, the solution was diluted to 10 mL with water and filtered through a 0.45 μm membrane filter. The quantitative analysis of metals in the leaching solution was performed by ICP-MS.

Recovery of REEs from the leaching solution has been studied in dispersive SPE experiment using 5 mL of the diluted leaching solution and 50 mg of SiO_2-DPA. The suspension acidity was adjusted to pH = 3.0 and a total volume of 25 mL. The suspension has been stirred on a shaker for 30 min and centrifugated. Metal-containing adsorbent was further treated as it is described above for the desorption experiment. The concentration of metal ions has been determined by ICP-MS in the leaching solution, in the supernatant and the concentrate, obtained after REEs desorption.

Relative Enrichment factors (EF) of REEs were determined from Eq. (5).

$$EF = \frac{(\sum C_M^i)/C_{REEs}^i}{(\sum C_M^c)/C_{REEs}^c}, \quad (5)$$

where C_M^i, C_{REEs}^i, C_M^c and C_{REEs}^i- concentration of impurities (M) and REEs in the initial solution and the concentrate, correspondingly.

Samples of Eu and Tb-containing SiO_2-DPA were obtained by shaking 100 mg of the adsorbent with 10 mL of europium (III) or terbium (III) working solution (concentration $2 \cdot 10^{-5}$ mol L^{-1}) at pH = 3.0. The samples were shacked for about 2 h, then washed with Milli-Q water and dried at 120 °C under vacuum.

Statistical processing of the recovery data was carried out by means of a descriptive analysis summarizing mean values and standard deviations supported with the normality test of dispersion for an overall recovery value.

3. Results and discussion

3.1. The adsorbent preparation and quantitative characterization

Immobilization of the target 2,6-pyridinedicarboxylate ligand was performed by surface assembling. In such approach mesoporous silica was firstly modified with 3-aminopropyl-(triethoxysilane) (APTES), then aminosilica (SiO_2-NH_2) was treated with an excess of pyridine-2,6-dicarbonyl chloride in the presence of hindered amine and finally immobilized carbonyl chloride was hydrolyzed to carboxylic acid, as it is schematically demonstrated in Fig. 2. To increase the yield of the target ligand next procedure was strictly followed:

1. Prior modification mesoporous silica was dried at 500 °C to remove physically and chemically adsorbed water. Under this treatment isolated silanols mainly remain on silica surface;
2. APTES was used freshly distilled to remove partly hydrolyzed oligomers. The solvent used for APTES immobilization was water-free. These precautions reduce the probability of cluster-type topography of surface layer on SiO_2-NH_2 and thus high local density of immobilized groups;
3. A large excess of pyridine-2,6-dicarbonyl chloride was used to prevent the formation of arched structures, like those demonstrated in Fig. 1b,c.

The results of CHN analysis of SiO_2-DPA and pristane SiO_2-NH_2 are presented in Table S1 together with the calculation procedure used. These results allowed to demonstrate that SiO_2-DPA has 0.36 mmol g^{-1} of target dipicolinic and about 0.49 mmol g^{-1} of pristine propylamine fragments, Table 1.

The results of SiO_2-DPA chemical analysis were confirmed by TGA analysis of the adsorbent. The thermogram shows the significant weight loss of SiO_2-DPA at temperature > 300 °C, which corresponds to the thermal decomposition of the organic layer (ESI, Fig. S1). The pristine SiO_2-NH_2 also demonstrate weight loss, but significantly less than SiO_2-DPA. From this difference, the concentration of 2.6-pyridinedicarboxylic fragments was estimated as is described elsewhere (Alekseev et al., 2006). The results presented in Table 1 demonstrates good agreement between CHN and thermal analysis.

3.2. Characterization

Nitrogen adsorption/desorption experiment demonstrates that SiO_2-DPA has the N_2 adsorption/desorption isotherm identical to pristine SiO_2. This suggests that immobilization of 2.6-pyridinedicarboxylic fragments does not change the porous structure of silica support having typical Type IV isotherm with a distinct hysteresis loop of H1 within the p/p_0 range of 0.4–1.0, indicating mesopore presence. At high relative pressure, the saturation of the isotherms is clearly observed, and this feature indicates the complete filling of the mesopores and the absence of macropores. The pore size distribution on SiO_2-DPA has a single-mode profile (Fig. 3b). The textural parameters of SiO_2-DPA presented in Table 1 demonstrate that the average pore size of SiO_2-DPA is only slightly less than for the pristine silica. This is an indication that SiO_2-

Table 1
Material characterization results.

Material	Porosity Parameters					C_L[a], mmol g^{-1}	
	S_{BET}, m^2 g^{-1}	R_{ave}, nm		V_p, cm^3 g^{-1}		CHN[b]	TGA
		NLDFT	MND	NLDFT	MND		
SiO_2-DPA	389	3.5	3.9	0.564	0.581	0.36	0.35

[a] C_L - loading of functional groups;
[b] calculated from the mass fraction of nitrogen, as it is described in the ESI.

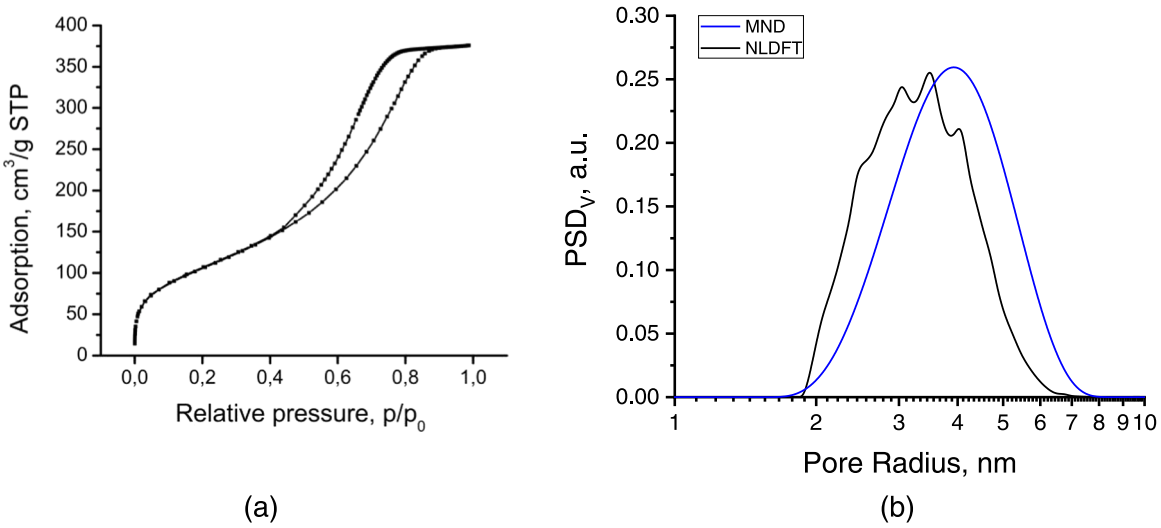

Fig. 3. Isotherm of nitrogen adsorption-desorption (a) and pore size distribution by volume computed with the help of NLDFT and MND methods (b) for SiO_2-DPA.

DPA has monolayer of covalently immobilized functional groups obtained by silylation of silica gel surface, rather by the silane hydrolysis (Zaitsev, 2003). This conclusion is indirectly confirmed by CHN analysis of SiO_2-NH_2 (Table S1).

Scanning electron microscopy images of unmodified silica gel and SiO_2-DPA demonstrated that the morphology of silica gel was not affected by any changes after manipulations attributed to the immobilization of 2,6-pyridinedicarboxylic acid (Fig. S2).

FTIR spectrum of SiO_2-DPA demonstrates essential changes in comparison with the spectrum of pristine SiO_2-NH_2, Fig. S3. Particularly, in addition to the bands, commonly observed for all silica-based materials, the spectrum of SiO_2-DPA demonstrates absorbance at 1646, 1546 cm^{-1}, that can be attributed to Amide-I and Amide-II bands, resulting from NHC=O stretching and C(O)-NH bending vibrations, correspondingly. Also, narrow peaks at 1420 cm^{-1} and 1450 cm^{-1} in FTIR of SiO_2-DPA are respectively attributed to the stretching vibration of C=C and C=N fragments of the pyridine ring. To this point, FTIR spectra confirm the anchoring of pyridine derivatives on aminosilica surface via acylation reaction, Fig. 2.

The survey XPS spectrum of SiO_2-DPA have bands attributed to the silica matrix elements (Si2p at 103.2 eV, Si2s at 154.3 eV and O1s at 532.5 eV), and immobilized organic fragments (C1s at 284.8 eV and N1s at 400.5 eV), Fig. 4.

Deconvoluted N1s band in high-resolution XPS of SiO_2-DPA consists of two components attributed to -NH_2 (399.7 eV) and C(O)-NH (401.9 eV) fragments, while SiO_2-NH_2 presented only one at 399.7 eV, with a small band at 401.6 commonly observed for SiO_2-NH_2 and attributed to -NH_3^+ groups, Fig. 5.

3.3. Adsorption properties of SiO_2-DPA

3.3.1. Effect of pH

The recovery of metal ions as a function of pH is a crucial parameter that demonstrates affinity of adsorbents to REEs because the pH affects both decompositions of the immobilized complexes and the speciation of metal ions in aqueous media. To eliminate the interference of $M(OH)_3$ precipitation and their chemisorption, the pH of the hydroxides precipitation was calculated based on solubility product constants (K_{sp}) for most common interfering ion (M = Fe, K_{sp} [$Fe(OH)_3$] = $6.3 \cdot 10^{-38}$ and one of the target ion (M = La, K_{sp}[$La(OH)_3$] = $2.0 \cdot 10^{-21}$) ("CRC Handbook of Chemistry and Physics 100th Edition," n.d.). Based on the K_{sp} calculations, the precipitation pH values for the metal concentration 10^{-3} mol L^{-1} were estimated as 2.93 (for $Fe(OH)_3$) and 7.2 (for $La(OH)_3$), Fig. 6. At pH above these values, the metal hydroxide precipitation is accompanied by the ion chemisorption. Taking to account that

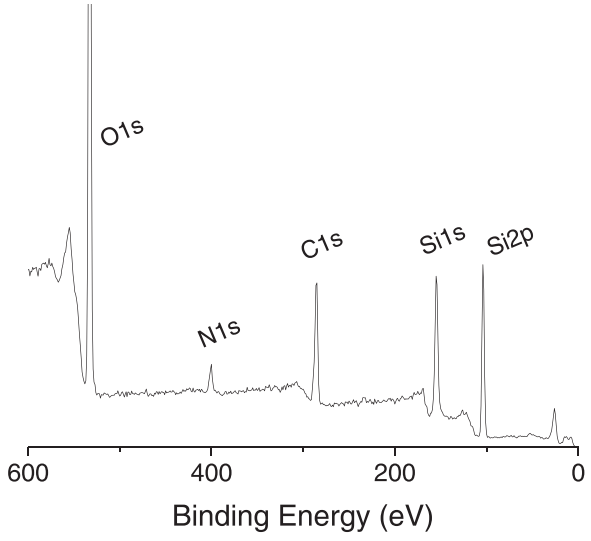

Fig. 4. Survey XPS general spectra of SiO_2-DPA.

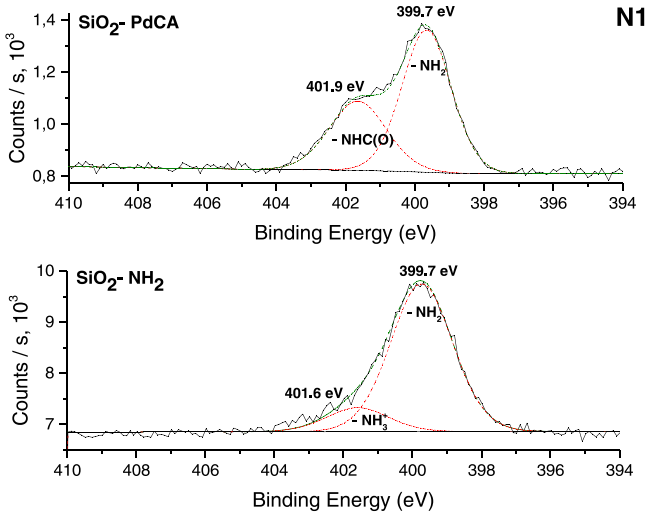

Fig. 5. XPS N1s spectra of SiO_2-DPA in comparison with SiO_2-NH_2.

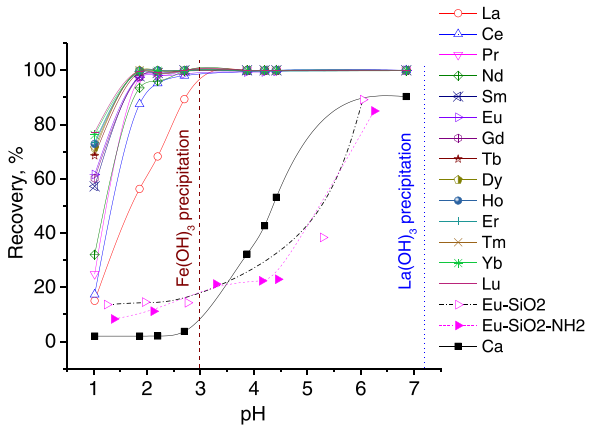

Fig. 6. Effect of pH on adsorption of 13 REEs ions on SiO_2-DPA, SiO_2 and SiO_2-NH_2. Experimental conditions: the adsorbent weight 50 mg, each REE concentration 20.0 μg L^{-1}, Ca concentration 1.00 mg L^{-1}, suspension volume 10 mL, contact time 30 min.

REEs precipitation is observed at pH > 7.2, the chemisorption properties of SiO_2-DPA were investigated in the pH range 1.0–7.0, Fig. 6.

To study the specificity of REEs chemisorption on SiO_2-DPA a set of preliminary experiments were conducted to investigate their adsorption on silica gel and SiO_2-NH_2. As shown in Fig. 6, in the pH range from 1.0 to 5.5 adsorption of Eu (III), which was selected for demonstration purposes, on SiO_2 and SiO_2-NH_2 is essentially less than on SiO_2-DPA. SiO_2 and SiO_2-NH_2 also demonstrate the same low adsorption affinity towards other REEs, Fig. S4. In contrary, SiO_2-DPA has excellent adsorption properties and quantitively recover nearly all REEs ions from acidic solution within pH > 1.7, Fig. 6. It is important that SiO_2-DPA adsorbs REEs at pH smaller than pH of $Fe(OH)_3$ and $Al(OH)_3$ precipitation, which allows more effective separation of REEs from such abandoned ions as Fe(III) and Al(III). Another most common macro component of REE-containing minerals and e-waste is Ca. Fig. 6 demonstrates that adsorption of Ca ions on SiO_2-DPA in the pH range 1–3 is negligible.

An essential difference in adsorption properties of SiO_2-DPA towards REEs and Ca ions, as well as the low affinity of pristine SiO_2-NH_2 to REEs, confirm chemisorption of REEs on SiO_2-DPA due to their binding with immobilized 2,6-pyridinecarboxylate fragments. Further evidence of the formation of metal complexes on the adsorbent surface was obtained from investigation of photoluminescent properties of SiO_2-DPA samples treated by Eu and Tb salts and will be discussed later.

3.3.2. *Effect of contact time on metal adsorption*

The rate of metal adsorption has been studied for solution of Eu^{3+} with pH= 3.0 and initial concentration of metal 10 mg L^{-1}. Because SiO_2-DPA has open mesoporous structure and metal-binding sites are situated on the carrier surface, the metal adsorption on it is very fast, and almost finished in 5 min, Fig. 7.

The adsorption data were analyzed by pseudo-1st-order (6) and pseudo-2nd-order (7) models described by equations:

$$q_t = q_e\left(1 - e^{-k_1 t}\right), \tag{6}$$

$$q_t = \frac{k_2 q_e^2 t}{1 + k_2 q_e t}, \tag{7}$$

where t – time, min; q_e and q_t – adsorption capacity of metal ions at equilibrium and at time t (mg g^{-1}), k_1 - the rate constant of the pseudo-1st-order model (min^{-1}), k_2 - the rate constant of the pseudo-second-order model (g mg^{-1} min^{-1}).

The calculated kinetic parameters presented in Table 2 demonstrate that pseudo-second-order model better correlates with experimental

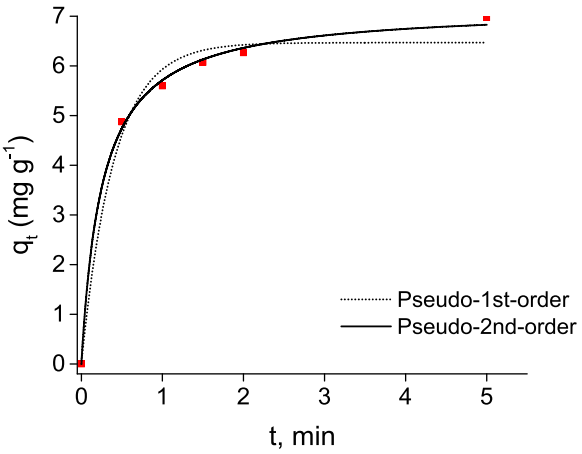

Fig. 7. The effect of the contact time on Eu^{3+} adsorption. Experimental conditions: adsorbent weight - 10 mg, initial metal concentration - 10.0 mg L^{-1}, suspension volume - 10 mL, pH 3.0.

Table 2
Kinetic parameters for Eu^{3+} adsorption.

Adsorbent	Pseudo-1st-order			Pseudo-2nd-order		
	q_e, mg g^{-1}	k_1, min^{-1}	R^2	q_e, mg g^{-1}	k_2, g mg^{-1} min^{-1}	R^2
SiO_2-DPA	6.47	2.49	0.979	7.18	0.543	0.997

data of Eu adsorption on SiO_2-DPA and thus metal ion diffusion into porous structure of the adsorbent does not limit the adsorption process.

Also, from kinetic parameters, it can be seen that adsorption of REEs on SiO_2-DPA is reached in minutes, while for chelating resins it can last for hours. These observations support the conclusion made above on monolayered immobilization of chelating groups on mesoporous surface silica and make silica-based adsorbent attractive for REE recovery.

3.3.3. *Adsorption isotherms*

Adsorption isotherm of Eu (III) on SiO_2-DPA was obtained for the metal solution with pH = 3.0. According to the results presented in Fig. 8, it can be attributed to H-type isotherm, suggesting strong chemisorption of REEs on SiO_2-DPA with quantitatively recover of Eu (III) from the solution.

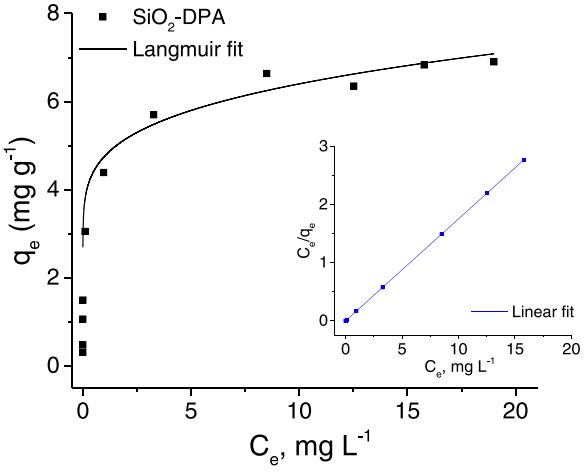

Fig. 8. Eu (III) adsorption isotherm on SiO_2-DPA and Langmuir linear fit (inset). Experimental conditions: adsorbent weight - 10 mg, metal concentration range - 0.1–25 mg L^{-1}, suspension volume - 10 mL, pH 3.0, contact time - 30 min.

The adsorption data were fitted on the basis of the Langmuir and Freundlich isotherm models. The linearized form of the Langmuir (8) or Freundlich (9) isotherm equations can be represented as:

$$\frac{1}{q_e} = \frac{1}{q} + \frac{1}{C_e}\frac{1}{qK_L}, \quad (8)$$

$$lnq_e = ln\,K_F + \frac{lnC_e}{n}, \quad (9)$$

where q_e - the amount of solute adsorbed (mg g^{-1}), C_e - equilibrium ion concentration in the solution (mg L^{-1}), q - saturated adsorption capacity (mg g^{-1}) and K_L - Langmuir adsorption constant (L mg^{-1}). n - Freundlich constant and K_F - binding energy constant reflecting the affinity of the adsorbents to metal ions (mg g^{-1}).

The adsorption behavior of Eu^{3+} on SiO_2-DPA has been better fitted by the Langmuir model, Table 3. This indicates the formation of a monolayer of the adsorbate, which correlates with a model of REEs chemisorption due to formation of metal complexes with immobilized 2,6-pyridinedicarboxylate derivatives.

3.3.4. The affinity of SiO_2-DPA

To investigate affinity of *SiO_2-DPA* toward REEs, metal distribution coefficients (K_d) were calculated for Henry region of the adsorption isotherms, using Eq. 3. The metal adsorption experiment was performed for multielement solution of REEs with pH 3.0 and the results were compared with similar experiments performed for SiO_2-NH_2 and SiO_2. The results presented in Fig. 9 demonstrate that K_d values for metal adsorption on SiO_2-DPA are in 10–15 times higher than on pristine silicas and reach values 10^4 mL g^{-1}. This observation demonstrates a high potential of SiO_2-DPA for quantitative recovery of REEs from acidic water solutions.

3.3.5. Adsorption and desorption cycles

Adsorption properties of SiO_2-DPA have been studied for the multielement solution of 14 REEs with pH = 3.0 at the conditions when essential excess of the binding sites is provided (Henry region of the adsorption isotherm). These conditions were selected to prevent non-specific co-precipitation of easy-hydrolyzed ions, such as Al(III) and Fe (III) at the higher pH, Fig. 6. Also, being strong chelating ligand, immobilized 2,6-pyridinedicarboxylate fragments can react with transition and post-transition metal ions (Fig. S5) which can result in the reduction of SiO_2-DPA capacity toward target REEs (Macauley and Hong, 1995; Zajtsev et al., 2004). The results of the investigation presented in Fig. 10a demonstrate that SiO_2-DPA quantitatively adsorbs all REEs in the selected conditions. Slight decrease in adsorption was observed for Ce, Pr and Gd ions, which can be explained by the lower stability of their complexes with immobilized ligands (Jernström et al., 2007).

Desorption of REEs from SiO_2-DPA has been investigated using solutions of HNO_3, EDTA and oxalic acid, Fig. S6. It was found that 2 mol L^{-1} water solution of HNO_3 demonstrates the best eluting properties, allowing to achieve complete (95–100%) elution of all REEs, Fig. 10b. This solution has been used in all further experiments for REEs desorption.

3.3.6. The adsorbent reusability

Reusability of the adsorbent has been studied in the course of ten adsorption/desorption cycles by evaluation of overall recovery of REEs.

Table 3
Adsorption isotherm parameters.

Adsorbent	Langmuir's isotherm model			Freundlich's isotherm model		
	q_{max}, mg g^{-1}	K_L, L mg^{-1}	R^2	K_F, mg g^{-1}	1/n	R^2
SiO_2-DPA	5.7	0.361	0.999	3.9	0.270	0.911

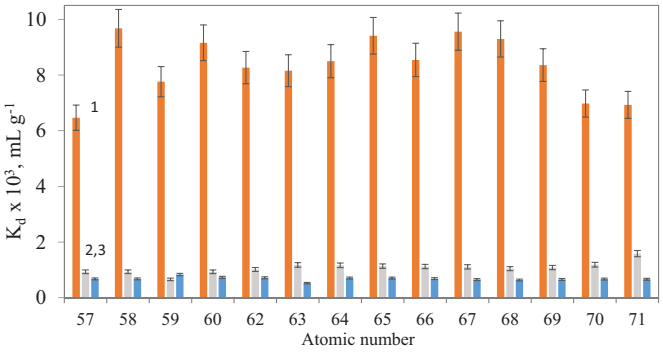

Fig. 9. Distribution coefficients (K_d) of REEs on SiO_2-DPA (1), SiO_2-NH_2 (2) and SiO_2 (3). Experimental conditions: adsorbent weight - 10 mg, initial metal concentration - 1.0 mg L^{-1}, suspension volume - 10 mL, pH 3.0, contact time – 30 min.

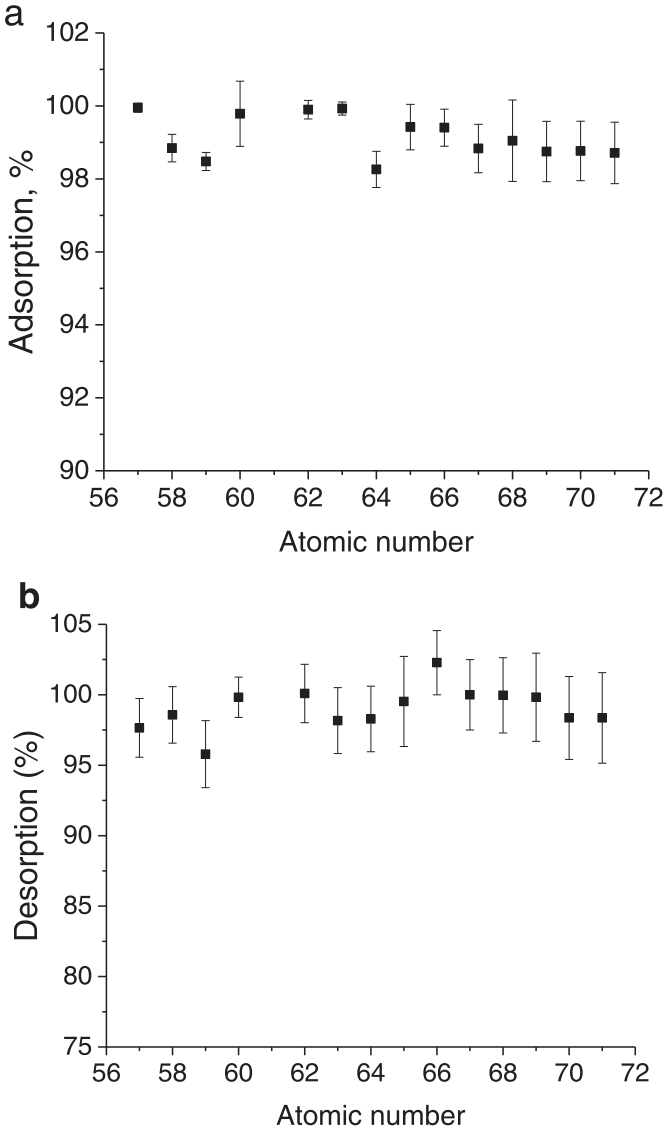

Fig. 10. Adsorption of REEs from multielement water solution in pH = 3.0 on SiO_2-DPA (a) and their desorption by 2 mol L^{-1} HNO_3 (b). Experimental conditions of adsorption: adsorbent weight - 10 mg, REEs concentration - 100.0 μg L^{-1} of each metal, suspension volume - 10 mL, contact time - 30 min. The data were obtained from five independent experiments.

The average value with upper and lower limits for all ten cycles is presented in Fig. 11.

From the results presented in Fig. 11, it can be seen that SiO_2-DPA can be successfully used for REEs recovery for at least in ten consecutive adsorption/desorption cycles with no noticeable loss of the adsorbent efficiency and with a mean value of REEs recovery larger than 97.8% (Table S3). From asymmetric distortion in upper and down parts of the violins it is clear that uncertainty of the recovery degree increases from light to heavy REEs, Fig. 11. It is probably related to incomplete desorption of heavy REEs in each cycle (see Fig. 10). Although the 95% confidence bars are available on the plots (Fig. 11), they demonstrate that a major part of the "violins" typically lies at the probability of 5%.

3.3.7. *The SiO_2-DPA selectivity*

Recovery of REEs on SiO_2-DPA was investigated in increased concentration of different foreign ions. Firstly, interference of Fe^{3+} and Cu^{2+} having a strong affinity to immobilized ligands (see Fig. S5) has been studied. The results presented in Fig. 12 demonstrate that generally speaking, recovery of REEs on SiO_2-DPA is decreased with increasing Cu and Fe concentration, but this decrease is essential for the recovery of La, Ce, Pr, Nd and Sm ions. For other REEs, even 3200-fold excess of Fe and Cu ions reduces REEs recovery only to 80–86%.

The second interfering solution used for investigation of SiO_2-DPA selectivity (solution B) was prepared in 0.5 mol L^{-1} NaCl and consists of three groups of ions: a) alkaline and alkaline earth metals (Li^+, Na^+, K^+, Mg^{2+}, Ca^{2+}, Sr^{2+} and Ba^{2+}); b) transition metal (Cr^{3+}, Mn^{2+}, Fe^{3+}, Co^{2+}, Ni^{2+}, Cu^{2+}, Ag^+), and c) post-transition metals (Zn^{2+}, Cd^{2+}, Al^{3+}, Ga^{3+}, In^{3+}, Tl^{3+}, Pb^{2+} and Bi^{3+}). Five samples of solution **B** with the concentration of each foreign ions from 1 mg L^{-1} to 16 mg L^{-1} have been added to SiO_2-DPA, while the concentration of each REE was kept constant (100 μg L^{-1}). The total concentration of the only transition and post-transition metal ions in solution **B** is up to 240 mg L^{-1}, which constitutes their 2400-fold excess to REEs ions. Therefore, solution B more essentially reduce REEs recovery than solution A, Fig. 13. Similar to solution A, recovery of light REEs (and particularly La and Ce) from solution B falls up to 8–9%. Nevertheless, the recovery of heavy REEs (from Eu to Lu) declines only on 20–30%, Fig. 13.

These experiments demonstrate the great potential of SiO_2-DPA to recover REEs even from complex solutions having large excess of transition and post-transition metals and high concentration (at least 30 g L^{-1}) of NaCl.

High selectivity noticed for SiO_2-DPA can be explained by complexation of immobilized derivatives of 2,6-pyridinecarboxylic acid with REEs. This statement is supported by the results obtained from the investigation of photoluminescent properties of SiO_2-DPA treated by Eu and Tb ions.

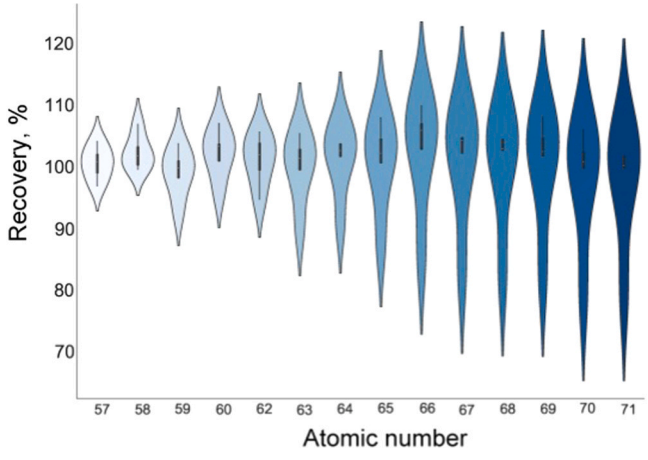

Fig. 11. The violin plots on the recovery of REEs on SiO_2-DPA from multielement water solution in pH= 3.0 with further desorption by 2 mol L^{-1} HNO_3 in ten adsorption-desorption cycles.

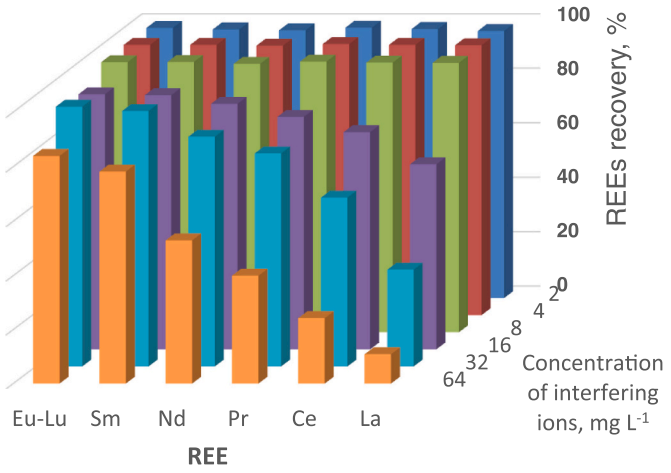

Fig. 12. Recovery of REEs by SiO_2-DPA from solutions containing different concentration (from 1 to 64 mg L^{-1}) on interfering ions (Fe and Cu).

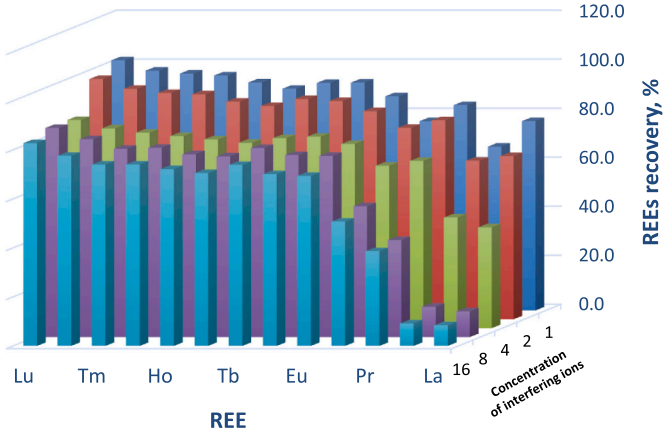

Fig. 13. Recovery of REEs by SiO_2-DPA from solutions containing different concentration (from 1 to 16 mg L^{-1}) on interfering ions of the solution B.

3.4. *Photoluminescent properties of immobilized Eu and Tb complex*

It is known that Eu and Tb ions form stable complexes with 2,6-pyridinedicarboxylic acid, which demonstrate strong red (Eu) and green (Tb) photoluminescence (PL) (Maji et al., 2015). To prove that adsorption of REEs from water solution is observed due to their complexation with immobilized ligands, PL spectra of Tb^{3+} and Eu^{3+} containing samples of SiO_2-DPA were investigated. For this, the adsorbent was immersed into a water solution of corresponding salts with pH = 3.0 and, after 15 min of contact, the precipitate was separated by decantation, washed with water several times and dried in vacuum at room temperature. It was found that resulted in solids emit visible by necked eye red (for Eu) and green (for Tb) light under illumination with UV-lamp, Fig. 14.

The 3D PL emission spectra of Eu and Tb-containing SiO_2-DPA excited within the 4–6 eV energy at room temperature confirm that photoluminescence of the solids is due to electron transitions in F-elements. Fig. 14.

Indeed, after adsorption of Eu^{3+} or Tb^{3+} ions, silica composites demonstrate strong luminescent emissions between 480 and 650 nm, that can be attributed to 4 f → 4 f transitions of the $^5D_0$ excited state to the low-lying ^7F_J (J = 0, 1, 2, 3, 4) levels of Eu^{3+} ions and $^5D_4 \rightarrow {}^7F_n$ (n = 3, 4, 5, 6) electron transitions of the Tb^{3+} ions. No emission peaks

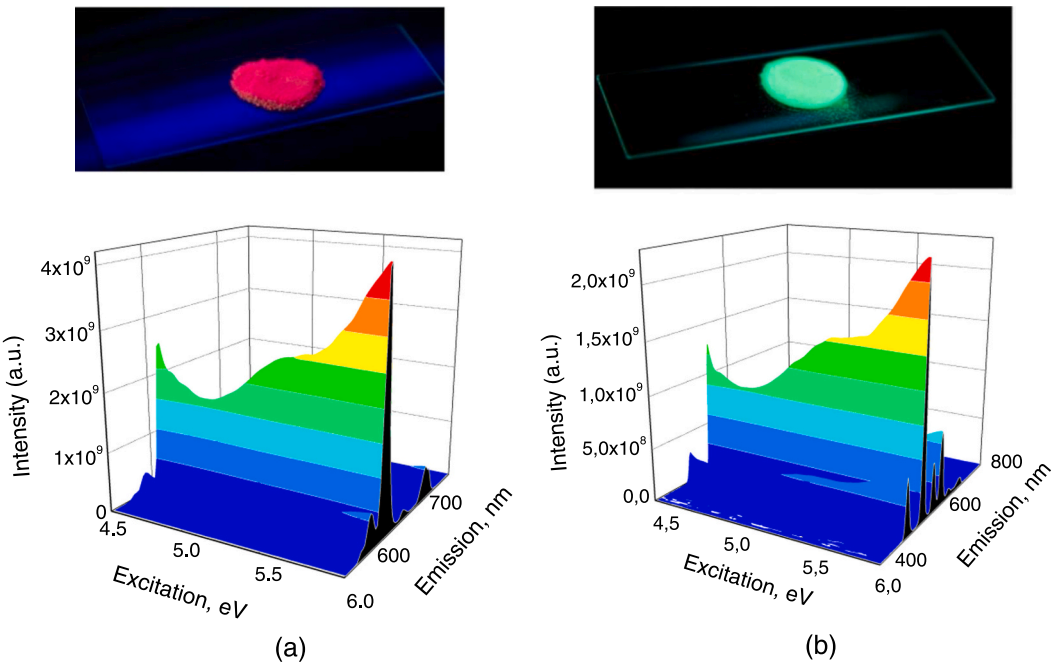

Fig. 14. Photo and 3D mapping of PL spectra for of SiO_2-DPA samples treated by Eu (a) and Tb (b) ions.

from the ligands were observed under this excitation.

Example of 2D emission spectra of Eu and Tb containing SiO_2-DPA are shown in Fig. 15.

Regardless that spectra were recorded for solid samples at room temperature, they demonstrate well-separated emission peaks, which allowed to determine the composition and geometry of immobilized metal species. For example, PL spectrum of SiO_2-DPA-Eu is very similar to individual Eu complex with 2,6-pyridinedicarboxylate (DPA), Na[Eu(DPA)$_3$] (Murray et al., 1990). Particularly, PL spectrum of SiO_2-DPA-Eu has no peak for forbidden $^5D_0 \rightarrow {}^7F_0$ transitions, peak attributed to $^5D_0 \rightarrow {}^7F_3$ forbidden transition at 650 nm is very weak, $^5D_0 \rightarrow {}^7F_1$ and $^5D_0 \rightarrow {}^7F_4$ transitions can be deconvoluted into two peaks each, while $^5D_0 \rightarrow {}^7F_2$ is the strongest one and has only one component, Fig. 15. The presence of $^5D_0 \rightarrow {}^7F_2$ transitions of Eu^{3+} and $^5D_4 \rightarrow {}^7F_5$ of Tb^{3+} reveals that metal adsorption on SiO_2-DPA takes place due to the formation of the metal complexes with immobilized derivatives of 2,6-pyridinedicarboxylic acid, as it is schematically demonstrated in Fig. 16.

3.5. Recovery of REEs from leaching solution of waste fluorescent lamps

SiO_2-DPA was applied for the recovery of REEs from the waste of fluorescent lamps. The waste fluorescent powder was collected from tubular lamps of various types and manufacturers. After adjustment of pH, the adsorbent was immersed to the leaching solution, then separated by centrifugation and rinsed and, finally, the eluting solution was added. The concentration of metals was determined in the leaching and eluting solutions, as well as in supernatant. According to the multielement analysis of the leaching solution (Table S2) it consists of alkaline, alkaline earth, transition and post-transition metals, and particularly: Ca (84%), Na (5%), Al (5%), Mn (1.54%), Sb (1.73%) and only 0.02% of REEs, Fig. 17a. Application of SiO_2-DPA allowed essential changes in the composition of the target solution. First of all, its total salinity drops down to 0.07 g L^{-1} (4.6 g L^{-1} for leaching solution). The concentration of alkaline earth ions decreased 4000–200 times; Mn and Al 500 times, Fe and Sb 100–57 times, while losses of REEs in the leaching solution were less than 17%, Table S2. The leaching solution mainly consists of Na (29%), Zn (21%), Sb (12%) and REEs (12%), Fig. 17b. Application of

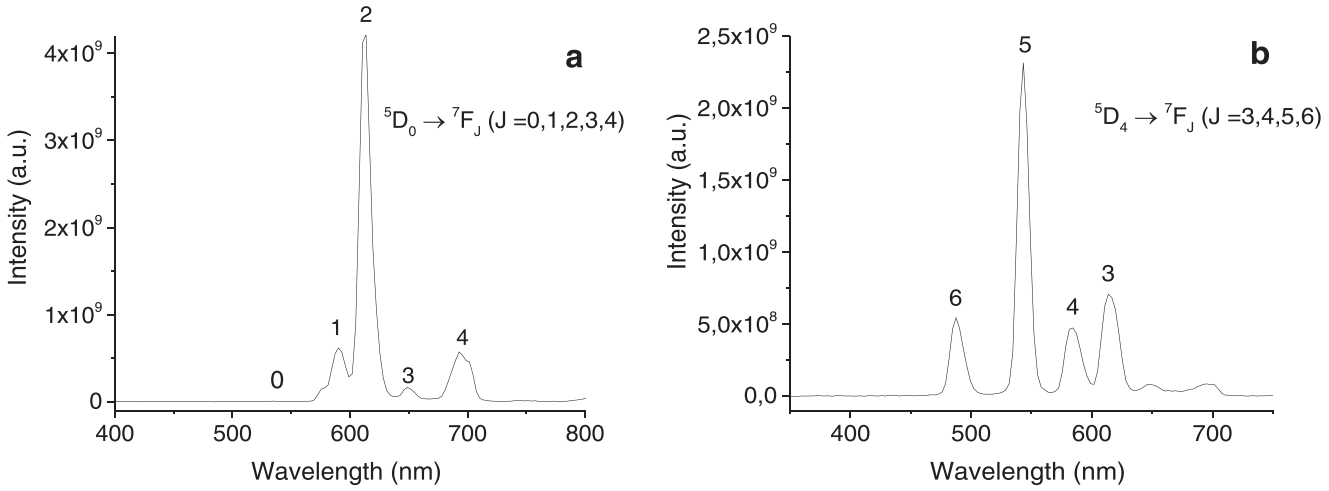

Fig. 15. PL spectra of SiO_2-DPA-Eu (a) and SiO_2-DPA-Tb (b).

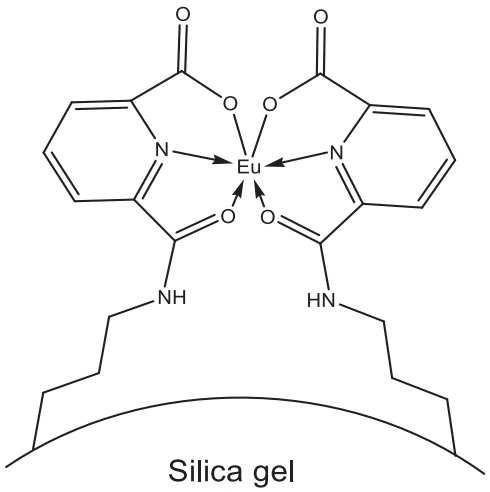

Fig. 16. Schematic structure of Eu complexes with fragments of immobilized 2,6-pyridinedicarboxylic acid.

SiO_2-DPA allowed to recover 83% of REEs from acidic leaching solution of fluorescent lamp waste, with enrichment factor ER= 615.

From the concise results of REEs determination shown in Table 4, it can be seen that recovery of almost all REEs is above 80%, only the recovery of La decreases to 50%, similarly to results obtained for model solutions (see Fig. 13).

It is important to mention that, regardless of the essential difference in composition of leaching and eluting solutions, distribution of the recovered REEs is almost identical to its initial distribution in the leaching solution, Fig. 18. This fact confirms the appropriateness of the sample preparation procedure and precisions of the analysis.

4. Conclusions

Mesoporous silica functionalized with fragments of dipicolinic acid was shown to be highly effective in adsorbing lanthanides from the synthetic solution containing a large excess of transition and post-transition ions and from real leaching solution from the waste of fluorescent lamps. SiO_2-DPA is capable for quantitative adsorption of REE from acidic solution with pH > 1.7, while adsorption of transition metals is observed at lower acidity. Due to this effect adsorption of macro-components of the leaching solution such as Na, Ca, Mg, Ba, Sr, Mn, Al and Sb has no or little influence on REEs recovery. Thus SiO_2-DPA can be used for recycling of REE from e-waste. Complete elution of adsorbed REE was achieved with 2.0 mol L^{-1} HNO_3, with no degradation in adsorbent performance over multiple reuse cycles.

CRediT authorship contribution statement

Olena Artiushenko: Methodology, Investigation, Writing - original

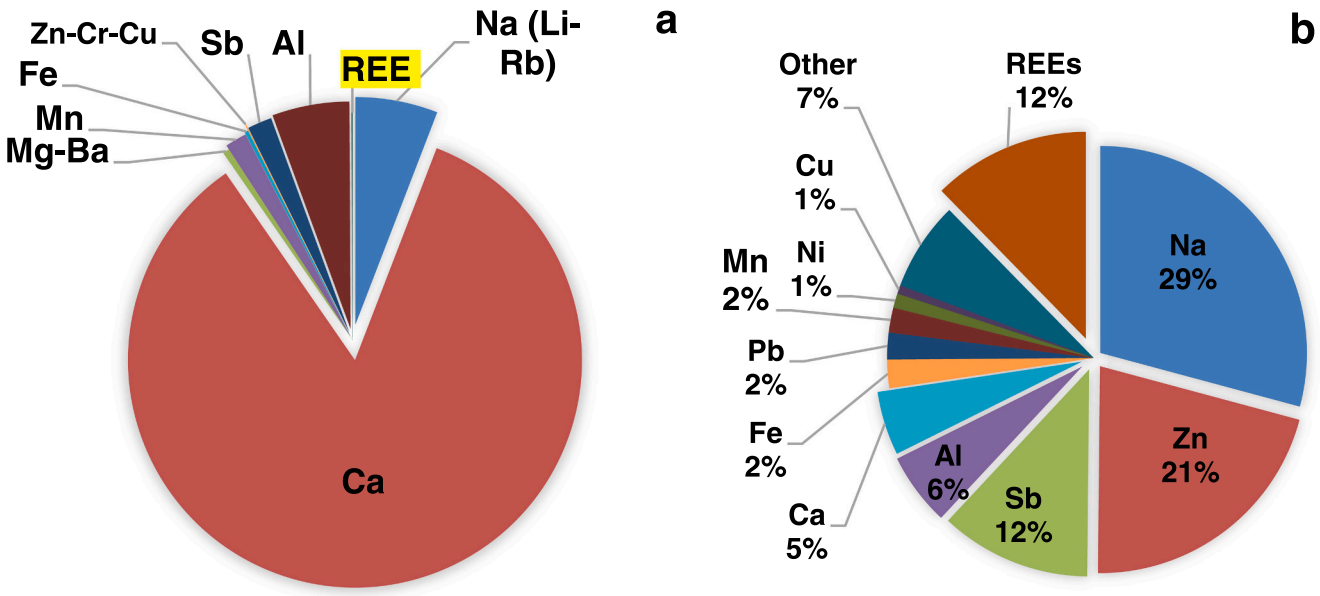

Fig. 17. Distribution of metal ions in the leaching (a) and the eluting (b) solutions.

Table 4
The results of REEs determination in the leaching solution obtained from waste fluorescent lamps.

REE	determined in the leaching solution, mg L^{-1}	determined in the supernatant mg L^{-1}	degree of adsorption, %	determined in the eluting solution, mg L^{-1}	Recovery, %
Y	0.39	<0.01	>96	0.33	80
Eu	0.17	<0.005	>96	0.15	85
Tb	0.15	<0.003	>98	0.12	79
Yb	0.12	<0.002	>98	0.085	67
La	0.014	<0.005	>67	0.011	52
Gd	0.077	<0.002	>98	0.067	85
Sm	0.051	<0.002	>97	0.046	87
Nd, Ce, Er	<0.030	<0.002	100–92	0.03–0.025	68–93
Dy, Pr, Ho, Tm, Lu	<0.005	<LOD	100	0.005–0.002	83–90
REEs total	1.069			0.887	83%

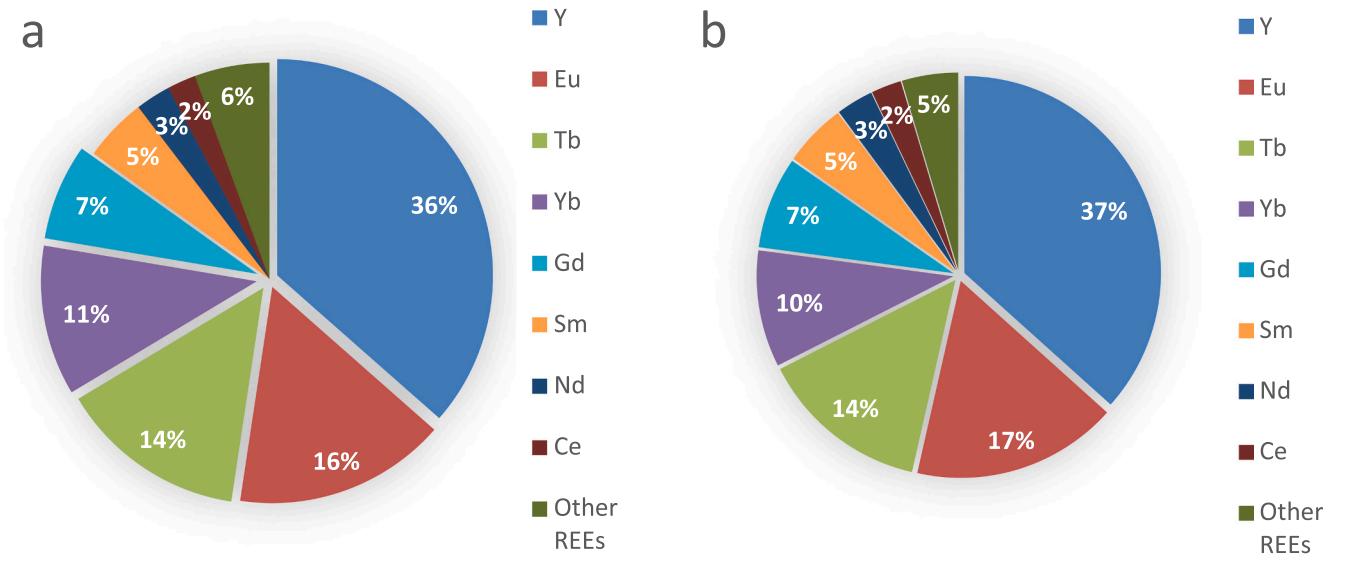

Fig. 18. Distribution of REEs ions in the leaching (a) and the eluting (b) solutions.

draft. **Vladimir Zaitsev**: Conceptualization, Supervision, Writing - original draft, Writing - review & editing. **Wendy S. Rojano**: Investigation. **Gabriel A. Freitas**: Investigation. **Michael Nazarkovsky**: Software, Visualization, Writing - review & editing. **Tatiana D. Saint'Pierre**: Data curation, Formal analysis. **Jiang Kai**: Conceptualization, Writing - review & editing.

Declaration of Competing Interest

The authors declare that they have no known competing financial interests or personal relationships that could have appeared to influence the work reported in this paper.

Acknowledgments

This study was financed in part by the Coordenação de Aperfeiçoamento de Pessoal de Nível Superior - Brasil (CAPES) - Finance Code 001. The authors are thankful to the National Council for Scientific and Technological Development (CNPq), Grants 401383/2014-8, 311820/2017-4 and 304622/2015-0 and Fundação Carlos Chagas Filho de Amparo à Pesquisa do Estado do Rio de Janeiro (FAPERJ), grants E-26/210.547/2019, E-26/010.978/2019 for the financial support. This research used resources of the Brazilian Synchrotron Light Laboratory (LNLS), an open national facility operated by the Brazilian Center for Research in Energy and Materials (CNPEM) for the Brazilian Ministry for Science, Technology, Innovations and Communications (MCTIC). The TGM beamline staff is acknowledged for assistance during the experiments. The authors acknowledge technical assistance of Brazilian Nanotechnology National Laboratory (LNNano) in the XPS study.

Appendix A. Supporting information

Supplementary data associated with this article can be found in the online version at doi:10.1016/j.jhazmat.2020.124976.

References

Alekseev, S.A., Zaitsev, V.N., Fraissard, J., 2006. Organosilicas with covalently bonded groups under thermochemical treatment. Chem. Mater. 18, 1981–1987. https://doi.org/10.1021/cm052776a.

Ambaye, T.G., Vaccari, M., Castro, F.D., Prasad, S., Rtimi, S., 2020. Emerging technologies for the recovery of rare earth elements (REEs) from the end-of-life electronic wastes: a review on progress, challenges, and perspectives. Environ. Sci. Pollut. Res. 27, 36052–36074. https://doi.org/10.1007/s11356-020-09630-2.

Artiushenko, O., Ávila, E.P., Nazarkovsky, M., Zaitsev, V., 2020a. Reusable hydroxamate immobilized silica adsorbent for dispersive solid phase extraction and separation of rare earth metal ions. Sep. Purif. Technol. 231. https://doi.org/10.1016/j.seppur.2019.115934.

Artiushenko, Olena, Kostenko, L., Zaitsev, V., 2020b. Influence of competitive eluting agents on REEs recovery from silica gel adsorbent with immobilized aminodiphosphonic acid. J. Environ. Chem. Eng. 8, 103883 https://doi.org/10.1016/j.jece.2020.103883.

Barja, B.C., Bari, S.E., Marchi, M.C., Iglesias, F.L., Bernardi, M., 2011. Luminescent Eu (III) hybrid sensors for in situ copper detection. Sens. Actuators B Chem. 158, 214–222. https://doi.org/10.1016/j.snb.2011.06.006.

Binnemans, K., Jones, P.T., Blanpain, B., Van Gerven, T., Yang, Y., Walton, A., Buchert, M., 2013. Recycling of rare earths: a critical review. J. Clean. Prod. 51, 1–22. https://doi.org/10.1016/j.jclepro.2012.12.037.

Callura, J.C., Perkins, K.M., Noack, C.W., Washburn, N.R., Dzombak, D.A., Karamalidis, A.K., 2018. Selective adsorption of rare earth elements onto functionalized silica particles. Green Chem. 20, 1515–1526. https://doi.org/10.1039/C8GC00051D.

Cardoso, C.E.D., Almeida, J.C., Lopes, C.B., Trindade, T., Vale, C., Pereira, E., 2019. Recovery of rare earth elements by carbon-based nanomaterials—a review. Nanomaterials 9. https://doi.org/10.3390/nano9060814.

Cardoso, Celso E.D., Almeida, J.C., Lopes, C.B., Trindade, T., Vale, C., Pereira, E., 2019b. Recovery of rare earth elements by carbon-based nanomaterials—a review. Nanomaterials 9, 814. https://doi.org/10.3390/nano9060814.

Chour, Z., Laubie, B., Morel, J.L., Tang, Y., Qiu, R., Simonnot, M.-O., Muhr, L., 2018. Recovery of rare earth elements from Dicranopteris dichotoma by an enhanced ion exchange leaching process. Chem. Eng. Process. Process Intensif. 130, 208–213. https://doi.org/10.1016/j.cep.2018.06.007.

CRC Handbook of Chemistry and Physics 100th Edition [WWW Document], n.d. http://hbcponline.com/faces/contents/ContentsSearch.xhtml.

Dushyantha, N., Batapola, N., Ilankoon, I.M.S.K., Rohitha, S., Premasiri, R., Abeysinghe, B., Ratnayake, N., Dissanayake, K., 2020. The story of rare earth elements (REEs): occurrences, global distribution, genesis, geology, mineralogy and global production. Ore Geol. Rev. 122. https://doi.org/10.1016/j.oregeorev.2020.103521.

Dutta, T., Kim, K.-H., Uchimiya, M., Kwon, E.E., Jeon, B.-H., Deep, A., Yun, S.-T., 2016. Global demand for rare earth resources and strategies for green mining. Environ. Res. 150, 182–190. https://doi.org/10.1016/j.envres.2016.05.052.

Engelhardt, H., 1979. High Performance Liquid Chromatography, Chemical Laboratory Practice. Springer, Heidelberg. https://doi.org/10.1007/978-3-642-67064-0.

European Commission, 2017. Communication from the commission to the European Parliament, the council, the European Economic and Social Committee and the Committee of the Regions on the 2017 list of Critical Raw Materials for the EU COM/2017/0490 final [WWW Document]. Doc. 52017DC0490. https://eur-lex.europa.eu/legal-content/EN/TXT/?uri=CELEX:52017DC0490 (Accessed 6 November 2020).

Franville, A.-C., Mahiou, R., Zambon, D., Cousseins, J.-C., 2001. Molecular design of luminescent organic-inorganic hybrid materials activated by europium (III) ions. Solid State Sci. 3, 211–222. https://doi.org/10.1016/S1293-2558(00)01114-6.

Gaustad, G., Williams, E., Leader, A., 2020. Rare earth metals from secondary sources: review of potential supply from waste and byproducts. Resour. Conserv. Recycl., 105213 https://doi.org/10.1016/j.resconrec.2020.105213.

Gergoric, M., Ekberg, C., Foreman, M.R.S.J., Steenari, B.-M., Retegan, T., 2017. Characterization and leaching of neodymium magnet waste and solvent extraction of the rare-earth elements using TODGA. J. Sustain. Metall. 3, 638–645. https://doi.org/10.1007/s40831-017-0122-8.

Gun'ko, V.M., 2014. Composite materials: textural characteristics. Appl. Surf. Sci. 307, 444–454. https://doi.org/10.1016/j.apsusc.2014.04.055.
Hu, B., He, M., Chen, B., Jiang, Z., 2016. Separation/preconcentration techniques for rare earth elements analysis. Phys. Sci. Rev. 1. https://doi.org/10.1515/psr-2016-0056.
Hu, Y., Florek, J., Larivière, D., Fontaine, F.-G., Kleitz, F., 2018. Recent advances in the separation of rare earth elements using mesoporous hybrid materials. Chem. Rec. 18, 1261–1276. https://doi.org/10.1002/tcr.201800012.
Iftekhar, S., Ramasamy, D.L., Srivastava, V., Asif, M.B., Sillanpää, M., 2018. Understanding the factors affecting the adsorption of Lanthanum using different adsorbents: a critical review. Chemosphere 204, 413–430. https://doi.org/10.1016/j.chemosphere.2018.04.053.
Jernström, J., Lehto, J., Betti, M., 2007. On-line separation of Pu(III) and Am(III) using extraction and ion chromatography. J. Radioanal. Nucl. Chem. 274, 95–102. https://doi.org/10.1007/s10967-006-6909-x.
Jyothi, R.K., Thenepalli, T., Ahn, J.W., Parhi, P.K., Chung, K.W., Lee, J.-Y., 2020. Review of rare earth elements recovery from secondary resources for clean energy technologies: grand opportunities to create wealth from waste. J. Clean. Prod. 267, 122048 https://doi.org/10.1016/j.jclepro.2020.122048.
Karadaş, C., Kara, D., Fisher, A., 2011. Determination of rare earth elements in seawater by inductively coupled plasma mass spectrometry with off-line column preconcentration using 2,6-diacetylpyridine functionalized Amberlite XAD-4. Anal. Chim. Acta 689, 184–189. https://doi.org/10.1016/j.aca.2011.01.049.
Landers, J., Gor, G.Y., Neimark, A.V., 2013. Density functional theory methods for characterization of porous materials. Colloids Surf. A Physicochem. Eng. Asp. 437, 3–32. https://doi.org/10.1016/j.colsurfa.2013.01.007.
Lerner, N., Meyerstein, D., Shamir, D., Marks, V., Shamish, Z., Ohaion-Raz, T., Maimon, E., 2019. A chemically modified silica-gel as an ion exchange resin for pre-concentration of actinides and lanthanides. Inorg. Chim. Acta 486, 642–647. https://doi.org/10.1016/j.ica.2018.11.018.
Li, Z., Zhou, J.-J., Zuo, S.-Y., Yuan, X., Ma, C.-C., Song, Y.-S., Zhang, H., 2015. Synthesis of lanthanide-based SBA-15 mesoporous hybrids by a novel route. Chem. Pap. 69. https://doi.org/10.1515/chempap-2015-0172.
Macauley, E., Hong, A., 1995. Chelation extraction of lead from soil using pyridine-2,6-dicarboxylic acid. J. Hazard. Mater. 40, 257–270. https://doi.org/10.1016/0304-3894(94)00087-W.
Maji, S., Kumar, S., Sankaran, K., 2015. Fluorescence and co-fluorescence of Tb3+ and Eu3+ in acetonitrile using 2,6-pyridine dicarboxylic acid as ligand. Spectrochim. Acta Part A Mol. Biomol. Spectrosc. 135, 405–409. https://doi.org/10.1016/j.saa.2014.07.022.
Mosai, A.K., Chimuka, L., Cukrowska, E.M., Kotzé, I.A., Tutu, H., 2019. The recovery of rare earth elements (REEs) from aqueous solutions using natural zeolite and bentonite. Water Air Soil Pollut. 230. https://doi.org/10.1007/s11270-019-4236-4.
Murray, G.M., Sarrio, R.V., Peterson, J.R., 1990. The effects of hydration on the luminescence spectra of trisodium tris(2,6-pyridinedicarboxylato)europium(III) compounds. Inorg. Chim. Acta 176, 233–240. https://doi.org/10.1016/S0020-1693(00)84849-5.
Noack, C.W., Perkins, K.M., Callura, J.C., Washburn, N.R., Dzombak, D.A., Karamalidis, A.K., 2016. Effects of ligand chemistry and geometry on rare earth element partitioning from saline solutions to functionalized adsorbents. ACS Sustain. Chem. Eng. 4, 6115–6124. https://doi.org/10.1021/acssuschemeng.6b01549.
Omodara, L., Pitkäaho, S., Turpeinen, E.-M., Saavalainen, P., Oravisjärvi, K., Keiski, R.L., 2019. Recycling and substitution of light rare earth elements, cerium, lanthanum, neodymium, and praseodymium from end-of-life applications - a review. J. Clean. Prod. 236, 117573 https://doi.org/10.1016/j.jclepro.2019.07.048.
Ottoni, M., Dias, P., Xavier, L.H., 2020. A circular approach to the e-waste valorization through urban mining in Rio de Janeiro, Brazil. J. Clean. Prod. 261, 120990 https://doi.org/10.1016/j.jclepro.2020.120990.Pagano, G., Thomas, P.J., Di Nunzio, A., Trifuoggi, M., 2019. Human exposures to rare earth elements: present knowledge and research prospects. Environ. Res. 171, 493–500. https://doi.org/10.1016/j.envres.2019.02.004.
Pereao, O., Bode-Aluko, C., Fatoba, O., Laatikaine, K., Petrik, L., 2018. Rare earth elements removal techniques from water/wastewater: a review. Desalin. Water Treat. 130, 71–86. https://doi.org/10.5004/dwt.2018.22844.
Pinta, T., 2017. Analytica Chimica Acta Selective solid phase extraction of lanthanides from tap and river waters with ion imprinted polymers 963, 44–52. https://doi.org/10.1016/j.aca.2017.02.012.
Pramanik, B.K., Nghiem, L.D., Hai, F.I., 2020. Extraction of strategically important elements from brines: Constraints and opportunities. Water Res 168. https://doi.org/10.1016/j.watres.2019.115149.
Pyrzynska, K., Kubiak, A., Wysocka, I., 2016. Application of solid phase extraction procedures for rare earth elements determination in environmental samples. Talanta 154, 15–22. https://doi.org/10.1016/j.talanta.2016.03.022.
Swain, N., Mishra, S., 2019. A review on the recovery and separation of rare earths and transition metals from secondary resources. J. Clean. Prod. 220, 884–898. https://doi.org/10.1016/j.jclepro.2019.02.094.
Verma, S., Dubey, A., 2020. 4-Chloro-2,6-pyridinedicarboxylic acid functionalized mesoporous silica nanocomposites for the synthesis of sinapaldehyde. Kinet. Catal. 61, 112–118. https://doi.org/10.1134/S0023158420010103.
Yuan, N., Liang, Y., Erichsen, E.S., Anwander, R., 2015. Lanthanide complex-incorporated periodic mesoporous organosilica nanospheres with tunable photoluminescence. RSC Adv. 5, 83368–83376. https://doi.org/10.1039/C5RA14694A.
Zaitsev, V.N., 2003. Chemically Modified Complexing Silicas: Predicting Analytical Applications Modified Silicas: Preconcentration, Separation, and Determination of Inorganic and Organic Compounds 58, 2003.
Zajtsev, V.N., Reva, T.D., Zajtseva, G.N., Alekseev, S.A., Kalibabchuk, V.A., 2004. The 2,6-pyridinedicarboxylic acid covalently bonded to the silochrome surface: immobilization and sorption-desorption properties. Ukr. Khimicheskij Zh. 70, 74–80.
Zhang, H., Mcdowell, R.G., Martin, L.R., Qiang, Y., 2016. Selective extraction of heavy and light lanthanides from aqueous solution by advanced magnetic nanosorbents. ACS Appl. Mater. Interfaces 8 (14), 9523–9531. https://doi.org/10.1021/acsami.6b01550.